Title

Combined spatiotemporal ICA (stICA) for continuous and dynamic lag structure analysis of MREG data

Authors

Ville Raatikainen[1,2], Niko Huotari[1], Vesa Korhonen[1,2], Aleksi Rasila[1], Janne Kananen[1,2], Lauri Raitamaa[1,2], Tuija Keinänen [2,3],Jussi Kantola[1], Osmo Tervonen[1,2], Vesa Kiviniemi[1,2]

Affiliations

[1] Department of Diagnostic Radiology, Medical Research Center (MRC), Oulu University Hospital, Oulu, Finland

[2] Research unit of Medical Imaging, Physics and Technology, the Faculty of Medicine, University of Oulu, Oulu, Finland

[3] Department of Clinical Neurophysiology, Oulu University Hospital, Oulu, Finland

Corresponding author

Ville Raatikainen, MSc (Tech.), Doctoral student

ville.raatikainen@oulu.fi

Department of Diagnostic Radiology, Medical Research Center (MRC), Oulu University Hospital

Kajaanintie 50, Oulu

Abbreviations

BOLD Blood oxygen level dependent
CO2 Carbon dioxide
DSC Dynamic susceptibility contrast
ECG Electrocardiography
EEG Electroencephalography
EPI Echo planar imaging
EVI Echo volumnar imaging
FFT Fast Fourier transform
fMRI Functional Magnetic Resonance Imaging
FOV Field of view
FSL FMRIB software library
IC Independent component
ICA Independent component analysis
INI Inverse imaging
GIN Generalized inverse imaging
DMN Default mode network
DMNpcc Posterior cingulate cortex default mode network
DMNvmpf Ventromedial default mode network
MCFLIRT Motion correction tool for fMRI time series
MEG Magnetoencephalography
M/EEG Magneto- and electroencephalography
MELODIC Multivariate exploratory linear optimized decomposition into independent components
MNI Montreal neurological institute
MPRAGE Magnetization-prepared rapid acquisition with gradient echo
MREG Magnetic resonance encephalography
NIBP Non-invasive blood pressure
NIRS Near-infrared spectroscopy
PSD Power spectral density
RSN Resting state networks
SD Standard deviation
sICA Spatial ICA
stICA Spatiotemporal independent component analysis
SpO2 Pulse oximeter oxygen saturation
TE Echo time
tICA Temporal ICA
TR Repetition time
VLFF Very low frequency fluctuations
VLF Very low frequency

ABSTRACT

This study investigated lag structure in the resting-state fMRI by applying a novel independent component (ICA) method to magnetic resonance encephalography (MREG) data. Briefly, the spatial ICA (sICA) was used for defining the frontal and back nodes of the default mode network (DMN), and the temporal ICA (tICA), which is enabled by the high temporal resolution of MREG (TR=100ms), was used to separate both neuronal and physiological components of these two spatial map regions. Subsequently, lag structure was investigated between the frontal (DMNvmpf) and posterior (DMNpcc) DMN nodes using both conventional method with all-time points and a sliding-window approach.

A rigorous noise exclusion criterion was applied for tICs to remove physiological pulsations, motion and system artefacts. All the de-noised tICs were used to calculate the null-distributions both for expected lag variability over time and over subjects. Lag analysis was done for the three highest correlating denoised tICA pairs.

Mean time lag of 0.6 s (± 0.5 std) and mean absolute correlation of 0.69 (± 0.08) between the highest correlating tICA pairs of DMN nodes was observed throughout the whole analyzed period. In dynamic 2 min window analysis, there was large variability over subjects as ranging between 1-10 sec. Directionality varied between these highly correlating sources an average 28.8% of the possible number of direction changes.

The null models show highly consistent correlation and lag structure between DMN nodes both in continuous and dynamic analysis. The mean time lag of a null-model over time between all denoised DMN nodes was 0.0 s and, thus the probability of having either DMNpcc or DMNvmpf as a preceding component is near equal. All the lag values of highest correlating tICA pairs over subjects lie within the standard deviation range of a null-model in whole time window analysis, supporting the earlier findings that there is a consistent temporal lag structure across groups of individuals. However, in dynamic analysis, there are lag values exceeding the threshold of significance of a null-model meaning that there

might be biologically meaningful variation in this measure. Taken together the variability in lag and the presence of high activity peaks during strong connectivity indicate that individual avalanches may play an important role in defining dynamic independence in resting state connectivity within networks.

Keywords:

spatiotemporal ICA | MREG | resting state fMRI | default mode network | lag structure | network dynamics

1 INTRODUCTION

The sources affecting spontaneous very low frequency fluctuations (VLFFs) of blood-oxygen-level dependent (BOLD) signal have remained unclear for over two decades (Biswal et al., 1995). Even though the VLFFs occur over the brain cortex with strong correlation to physiological variables, still independent signal sources having strong VLFFs present highest correlation within voxels of specific neurophysiological functional networks (Beckmann et al., 2005; Birn et al., 2006; Damoiseaux et al., 2006; Greicius et al., 2004; Kiviniemi et al., 2003).

Recent evidence with increased *temporal* resolution of combined magneto- and electroencephalography (M/EEG) recordings and magnetic resonance encephalography (MREG) suggest that the VLFF could be series of neuronal avalanches within functional network structures (Barbieri and Shimono, 2012; Liu and Duyn, 2013; Palva et al., 2013; Rajna et al., 2015; Tagliazucchi et al., 2011). Over several minutes subsequent avalanches are presented in a single voxel or a small ROI in temporal signal, but their dynamic spatial spread over time varies markedly from peak to peak (Rajna et al., 2015, Kiviniemi et al., 2011). The lag structure of the VLFFs over the whole brain has been extrapolated to be ~1 s with non-critically sampled TR 3 second BOLD data (Mitra et al., 2015a; Mitra et al., 2014). By studying temporal lags in the resting-state BOLD signal, it has been recently shown that spontaneous BOLD fluctuations consist of remarkably reproducible patterns of whole brain propagation (Mitra et al, 2015a). These consistent infra-slow lags have recently been observed using electrocorticograph (EcoG) (Mitra et al., 2016) and with optical imaging of gcamp6 in mouse models (Matsui et al., 2016). In addition, previous fMRI work has shown the temporal lag to be consistent across groups of individuals (Amemiya et al., 2016; Mitra et al., 2014).

According to Nyquist theorem a critical sampling rate has to be at least two times faster than the measured signal. If the measured signal is not critically sampled, the estimation of lag structure cannot be unequivocal but needs to be estimated by extrapolation of data (Mitra et al., 2014). This is not a trivial

matter since the brain was shown to present strong cardiorespiratory pulsations and ubiquitous very low frequency (VLF < 0.1 Hz) vasomotor waves propagate spatially over the whole brain. The cardiorespiratory pulsations aliases in classical TR > 400 ms BOLD signal (Kiviniemi et al., 2005; Kiviniemi et al., 2015; Majeed et al., 2011; Thompson et al., 2014; Thompson et al., 2015). Non-critically sampled pulsations in different frequencies also mix with natural motion artifacts, which will distort time signals in a unique pattern in each voxel and produce virtually un-recoverable signal changes in 2D echo planar imaging (EPI) data (Beall and Lowe, 2014). In addition to the previous problems the hemodynamic delay has been thought to vary significantly between distinct resting state networks (RSNs) and render causality/directionality analyses inaccurate (Biswal et al., 2003; Smith et al., 2011; Smith et al., 2012). In short, the separation of both neurovascular delay and electrophysiological lag in resting state data calls for both critically sampled signal and data driven analysis that offers spatiotemporally accurate way to separate signal sources simultaneously.

Independent component analysis (ICA) has been shown to separate sources linked to stable neuronal networks from functional magnetic resonance images (fMRI) of the brain (Beckmann et al., 2005; Calhoun et al., 2001; Damoiseaux et al., 2006; Esposito et al., 2005; Greicius et al., 2004; Kiviniemi et al., 2003; McKeown et al., 1998; van de Ven, Vincent G et al., 2004). ICA can be used in two ways, in spatial or in temporal domain. In temporal ICA (tICA) analysis temporal BOLD signal vector of each voxel serves as a source of density histograms for ICA, whereas in spatial ICA (sICA) all subsequent voxels per each brain volume form the histogram (Biswal and Ulmer, 1999; Calhoun et al., 2005; Jafri et al., 2008; McKeown et al., 1998). In classical 2-3 second TR BOLD fMRI data, sICA has been almost exclusively used; the whole brain coverage offers an order of magnitude larger histograms ensuring robust signal source estimation. Moreover, tICA of the whole brain data is often computationally intractable with classical BOLD due to relatively low number of time points.

While sICA can produce only one time signal per each separated spatial fMRI signal source, tICA can be used to give multiple temporal signals. In theory tICA can also be spatially overlapping and can nicely

represent the diversity of a given functional unit or area (Boubela et al., 2013; Smith et al., 2012). Recent study of 0.35 s TR BOLD, showed that tICA resting state networks are spatially nearly identical to sICA results and also present similar splitting of RSNs like default mode network (Boubela et al., 2013). There is an increasing tendency towards faster scanning, and some spatially still very accurate techniques are utilizing multiband acceleration schemes on conventional EPI (Chiew et al., 2015; Chiew et al., 2016; Narsude et al., 2015).

Even faster 3D imaging techniques like echo volumnar imaging (EVI) (Posse et al., 2013) and inverse imaging techniques like inverse imaging (InI), generalized inverse imaging (GIN) and MREG offer 0.1 s or less time resolution with whole brain coverage, which can critically sample both cardiac and respiratory pulsations (Assländer et al., 2013; Boyacioglu et al., 2013; Boyacioğlu and Barth, 2013; Lin et al., 2013; Lin et al., 2014). The inverse imaging techniques offers more time points for tICA density distributions in order to be both tractable computationally and accurate mathematically. Thus MREG allows sub-second lag structure estimation and robust differentiation of frequencies contributing to connectivity dynamics (Assländer et al., 2013; Lee et al., 2013; Posse et al., 2013). Estimation of lag can be made precise with ultra-fast imaging with results paralleling magnetoencephalography (MEG) results (Lin et al., 2013; Lin et al., 2014). Furthermore recent InI results suggest that the hemodynamic delay is not that variable and thus not a confounding major factor in lag analysis (Lin et al., 2013; Lin et al., 2014).

In this study we combine strengths of spatial and temporal ICA with ultrafast MREG data in order to obtain effective separation of resting-state neurophysiological and neurovascular signal sources within the default mode network. Spatial ICA was first used to separate functional RSN sources to minimize artefacts and the number of time vectors fed to tICA. Secondly, tICA was then used to obtain independent temporal signal sources. Our aim was to measure continuous and dynamic VLFF lag structure between ventromedial prefrontal (DMN_{vmpf}) and posterior cingulate cortex default mode network (DMN_{pcc}) with critically sampled MREG data.

2 MATERIALS AND METHODS

2.1 Subjects

Twenty-five healthy volunteers (15 males/10 females, mean age 24.8, SD 6.1 years) were imaged between years 2013 and 2015. Written informed consent was obtained from each subject prior to scanning, in accordance with the Helsinki declaration. The study protocol was approved by the ethical committee of Oulu University Hospital. During the 10 min MREG resting state study, subjects were instructed to lie still in the scanner with their eyes open fixating a cross in the screen and thinking nothing particular.

2.2 Measurements

Measurements were done using our novel multimodal imaging system – Hepta scan– that combines MREG, electroencephalography (EEG), non-invasive blood pressure (NIBP) and near-infrared spectroscopy (NIRS) with anesthesia monitor data (GE Datex-Ohmeda^{TM}; Aestiva/5 MRI) including respiration carbon dioxide ($respCO_{2)}$, peripheral capillary oxygen saturation ($SpO_{2)}$ and electrocardiography (ECG) (Korhonen et al., 2014). All data were accurately synchronized. The fMRI imaging was performed using Siemens 3T SKYRA scanner with a 32-channel head coil. We utilized MREG sequence obtained from Freiburg University via collaboration with Jürgen Hennig group (Lee et al., 2013; Zahneisen et al., 2012). MREG is a single-shot three dimensional (3D) sequence that utilizes spherical stack of spirals and undersamples 3D k-space trajectory (Assländer et al., 2013). It allows 20-25 times faster scanning than conventional fMRI by sampling the brain at the frequency of 10 Hz (TR=100 ms, TE=36 ms, and flip angle=25º, FOV=$(192\ mm)^3$, voxel size = $(3\ mm)^3$) . The data were reconstructed using L2-Tikhonov regularization with lambda=0.1, with the latter regularization parameter determined by the L-curve method (Hugger et al., 2011); an analysis of the point-spread function revealed that the resulting effective spatial resolution was 4.5 mm. Sampling rate of anesthesia monitor data was 300 Hz. In this study, MREG and anesthesia monitor data were utilized for analysis.

2.3 Pre-processing

MREG data were preprocessed with FSL pipeline (Jenkinson et al., 2012). The data were high-pass filtered with cut-off frequency of 0.0025 Hz (400 s) and one hundred eighty time points (18 s) were removed from the beginning of the data for minimizing T1-relaxation effects. Motion correction was performed using FSL MCFLIRT. Brain extraction was carried with FSL BET using the following parameters; fractional intensity=0.25, threshold gradient=0.22 with neck and bias-field correction option. Spatial smoothing was carried out using 5 mm FWHM Gaussian Kernel. MREG images were aligned to three-dimensional (MPRAGE) anatomical images in MNI152 standard space (full-search, 12 DOF) in 4 mm resolution prior to independent component analysis.

2.4 stICA workflow

The workflow of stICA is briefly presented in Figure 1 and is based on the following steps. Spatial ICA was run to the whole brain volume using FSL MELODIC's 'multi-session temporal concatenation' to define the uniform 70 independent components for all subjects. Here, two IC components, ventromedial prefrontal (DMN_{vmpf}) and posterior cingulate cortex default mode network (DMN_{pcc}), were selected for further study. Spatial ICA thresholded with z-score 3 produced 1444 voxels for DMN_{pcc} and 1828 for DMN_{vmpf}. The time series of voxels within DMN_{pcc} and DMN_{vmpf} ICs were chosen for tICA analysis.

Temporal ICA was carried out individually for each subject using FastICA algorithm (Hyvärinen and Oja, 1997). In FastICA data is centered and whitened before tICA,. All the vector components are uncorrelated and their variances equal unity after whitening process. Moreover, the dimensionalities of the data were reduced so that the dimension of the transformed data vector equals the number of independent components (Hyvärinen and Oja, 1997). Other used parameters were; approach=deflation, nonlinearity=tanh, stabilization=on. The restriction of the algorithm is that neither the signs or nor the energies of the independent components can be estimated (Hyvärinen and Oja, 1997). Nevertheless, FastICA algorithm provides a robust way to inspect the independent temporal patterns in the specific spatial area of the brain. TICA analysis was carried out using MATLAB software.

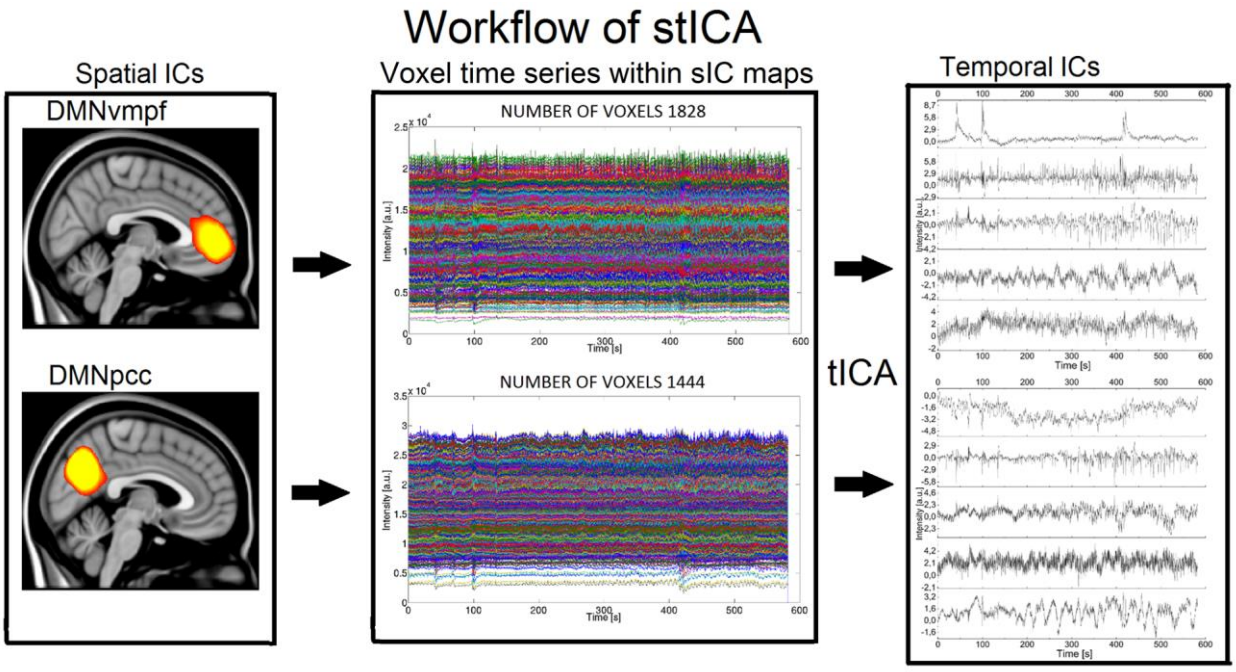

Figure 1. *General workflow of stICA. First, spatial ICA is run to the whole brain volume using FSL MELODIC's 'multi-session temporal concatenation' and two IC components* DMN_{vmpf} *and* DMN_{pcc} *are selected (lef box). The time series of voxels within* DMN_{vmpf} *and* DMN_{pcc} *IC maps that exceed the selected threshold (z>3) are chosen for tICA analysis. Right box presents example tICs of an individual subject.*

2.5 Experiment setup for analysis

Analyses were done for the first 7 minutes (4200 brain volumes) of the measurement. We decided to exclude the last 3 mins of 10 mins study since the data in three subjects had absent off-resonance correction in the image reconstruction during the last three minutes of the scanning. We selected model orders of 10, 30 and 50 tICA for analysis.

2.6 Identification and exclusion criteria for tICs

2.6.1 Exclusion of potentially motion affected tICs

MCFLIRT motion correction data of MREG measurements were used to exclude motion disrupted tICs. Velocity information was calculated by differentiating rotational and translational correction data in each x-, y- and z-dimension along time dimension. Separately, the absolute values of rotational and translational velocity data were summed in all three MNI spatial dimensions, resulting in a rotational and translational speed representation. The previous steps were done similarly with Rajna and co-workers (Rajna et al., 2015). Next, all tICs and eight motion signals were band pass filtered (0.009-0.1 Hz) and correlated. Temporal ICAs, having correlation > 0.25 with *any* of motion signals, were abandoned from the analysis.

2.6.2 Exclusion of the 1 Hz helium pump noise

Power spectral density (PSD) estimates using FFTs were calculated for each tIC. Next, trapezoidal numerical integration (trapz function in MATLAB) was performed for each tIC in the frequency band of 0.9976-1.0024 Hz. To exclude significant amount of helium pump noise from tICs, within each spatial ROI, the mean and standard deviation of trapz values were calculated from all tICs. Those tICs whose trapz value exceeded the sum of mean and standard deviation, were declared significant and thus excluded from the analysis.

2.6.3 Exclusion of cardiac and respiratory tICs

FFTs of SpO_2 and $respCO_2$ signals were calculated to verify cardiac and respiratory frequencies. From SpO_2, the frequency location of maximum magnitude in FFT was declared as cardiac frequency. Respiratory frequency was defined similarly from the FFT of $respCO_2$ signal. Seven subjects did not have a proper SpO_2 and $respCO_2$ signals. For those subjects we defined the respiratory and cardiac frequencies from the FFT of MREG sICA components. Next, frequency bands +/- 0.1 Hz were formed around both cardiac and respiratory frequencies. Using the PSDs calculated earlier, the trapezoidal numerical integration was calculated for both cardiac and respiration frequency bands. To exclude tICs with

significant respiratory information, within each spatial ROI, the mean and standard deviation of trapz values were calculated from all tICs. Those tICs whose trapz value exceeded the sum of mean and standard deviation, were declared significant respiratory tICs and thus excluded from the analysis. Cardiac tICs were excluded similarly, using the cardiac frequency band respectively.

2.6.4 Exclusion of tICs with significant warming effect

First order polynomial fitting was calculated for each tIC in the time range of first 120 s using polyfit function in MATLAB to define the regression slope coefficient. Based on the phantom test (see supplements), warming causes a raising (either raising or decreasing in ICA) curve in the MREG signal, i.e. large regression slope coefficient in the first 120 s of the measurement. This warming effect seems to be specific to MREG sequence. Within each spatial ROI, the mean and standard deviation of slope coefficient values were calculated from 50 tICs. Those tICs, whose slope coefficient value exceeded the sum of mean and 2 × standard deviation, were declared significant and thus excluded from the analysis.

2.7 Estimation of connectivity time lag between DMN_{vmpf} and DMN_{pcc} components

The remaining tICs that passed the exclusion criteria were detrended and bandpass filtered from 0.009 Hz to 0.1 Hz to estimate connectivity time lag. DMN_{vpmf} tICs were then correlated with DMN_{pcc} tICs. The three highest correlating signal pairs (nodes) were selected. Within the selected signal pair, the other signal was shifted sample by sample using +/- 100 sample range, i.e. 20 s time range and the time lag that gave the strongest correlation was declared as time lag between DMN front and back components (see Figure 2A). The absolute correlation in that specific time lag was listed as the corresponding correlation value in the results section. The connectivity lag estimates were calculated for each of the three nodes.

2.8 Estimation of connectivity dynamics

The highest correlating signal pairs were selected for the dynamics analysis. In recent studies it has been reported that the minimum window length to avoid the spurious fluctuations arising due to sliding window correlation itself should be at least equal to $1/f_{min}$, where f_{min} is the minimum frequency in the simplified correlating signal (Leonardi and Van De Ville, 2015; Shakil et al., 2015). Therefore, we selected the window length to be 120 s ($1/f_{min}$ = 111.1 s) with 60 s overlap by forming six time windows in the 7 mins long signal. In each of the six time windows, the other signal was shifted sample by sample using +/- 100 sample range (see Figure 2B), and the time lag and correlation giving the strongest absolute correlation were listed in the results section.

2.9. Null-distributions for correlation coefficients and time lags

The null model histograms for both correlation coefficients and time lags were formed from all denoised tICA pair values.

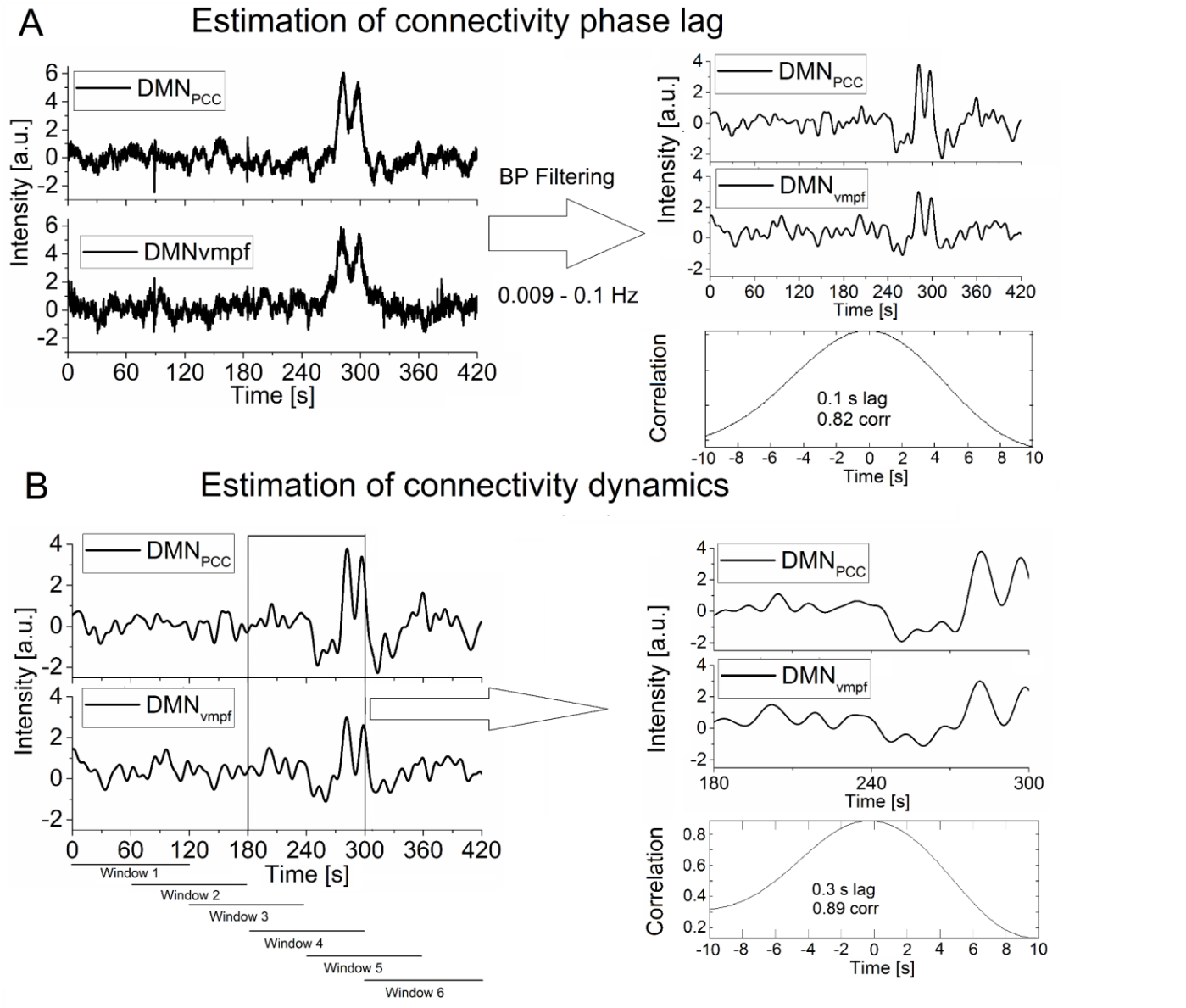

Figure 2. A. *Estimation of connectivity time lag. Once the best correlating tICs between two spatial ROIs (here* DMN_{pcc} *and* DMN_{vmpf}*) were selected after strict tICA exclusion criteria, the selected tICs were band pass filtered 0.009-0.1 Hz and then correlated. The other signal was shifted by sample +/- 100 samples, i.e. 10 s and the time lag that gave the strongest correlation was declared as time lag between DMN front and back components. The elevated activity is seen in both tICs.* ***B.*** *Estimation of connectivity dynamics. Connectivity dynamics calculations were applied to the best correlating and BP filtered (0.009-0.1 Hz) tICs in Figure 2A. We formed six time windows of 2 mins length and 1 mins overlap. In each time window the other signal was shifted by sample +/- 100 samples, i.e. 10 s and the time lag that gave the strongest correlation was declared as time lag between DMN front and back components.*

3 RESULTS

3.1 tICA signal overview

An example of tICA signals of DMN_{vmpf} of a single subject is illustrated in Figure 3. Cardiovascular pulses can be readily identified from sharp arterial type negative pulses. In distinction to venous/glymphatic pulsations, the arterial tICs have a sharper negative peak and present aortic valve notch, which emphasizes the 2^{nd} harmonic frequency in FFT spectrum (see Figure 3B). Respiratory tICs have a slower but rather regular sinusoidal signal fluctuation that corresponds to external respiration measurements.

Hardware warming effects present typical slow drift in the beginning of the scan, c.f. Supplementary Figure 1. Skyra helium pump presents a non-physiologically narrow 1 Hz power peak in FFT, cardiorespiratory peaks are wider due to physiological heart rate variability. Sudden motion tIC peaks can be correlated with FSL MCFLIRT motion estimates. More subtle MREG signal effects of motion were estimated from MCFLIRT motion parameters which were derivative into velocity estimates, both rotational and translational.

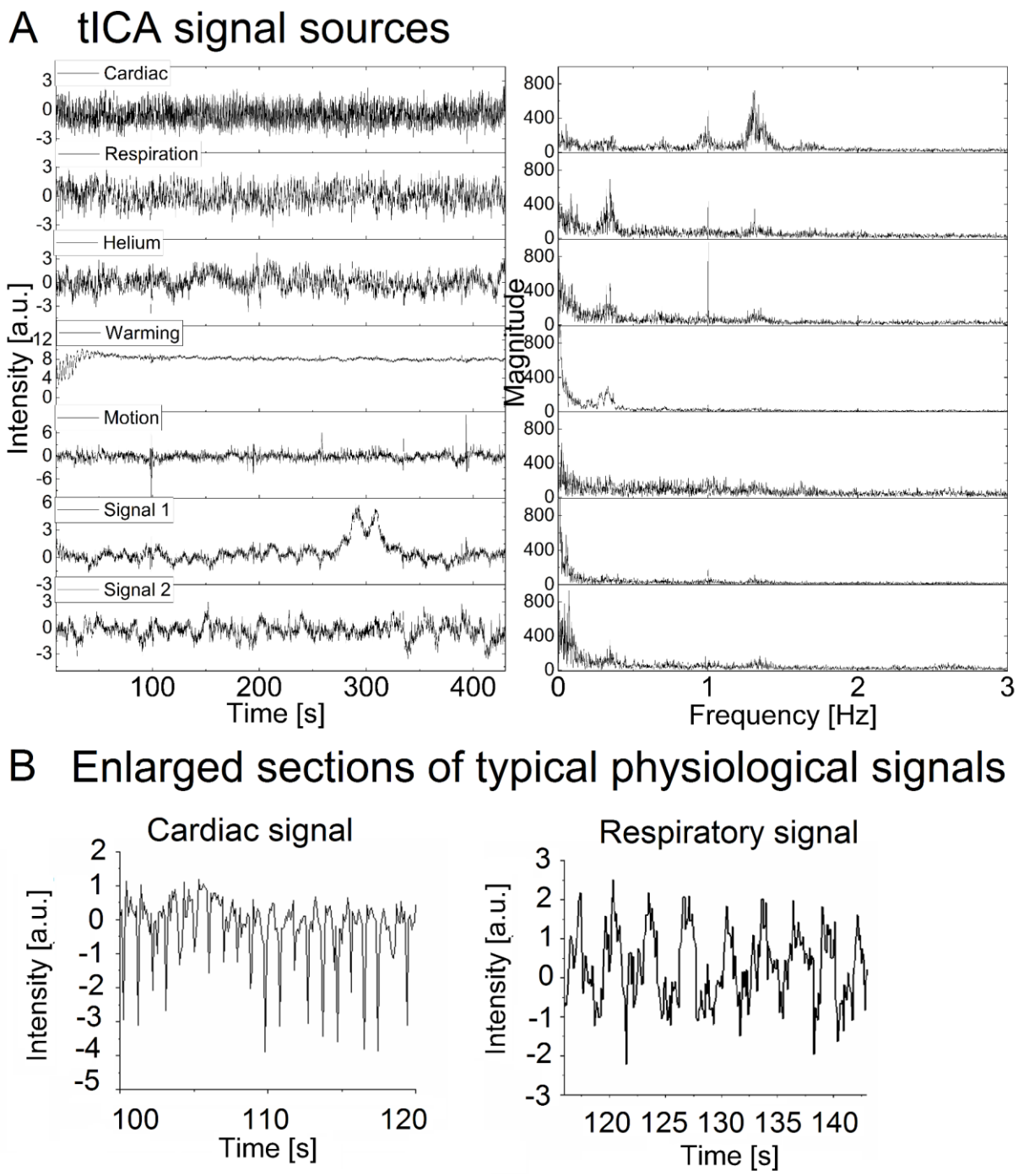

Figure 3. A. *Overview of signal sources of a single subject including time signals and corresponding FFTs is presented in Figure 7. Temporal ICs are named based on our identification and exclusion criteria (see section Identification and exclusion criteria for tICAs) referring to the most prominent feature (cardiac, respiration, helium, warming, motion and VLFF) in tICA. Signals 1 and 2 represent VLFF signals typical to RSN's as they have passed all exclusion criteria.* ***B.*** *Typical cardiac (above) and respiratory (bottom) signals of DMNvmpf calculated with stICA. The cardiac tIC includes a clear M-shape that is seen in the enlarged section (100-120 s) of the signal, presents the aortic closure wedge on the arterial pulse.*

3.2 Source separation vs. tICA model order

In order to estimate the effect of model order, we calculated 10, 30 and 50 tIC components from each dataset. The retained eigenvalues in ICA calculation explained roughly 94 % of the variance in 10 tICA, 98.5% in 30 tICA and 99.5% in 50 tICA.

Based on our tICA exclusion criteria (presented in section Identification and exclusion criteria for tICs), calculation of model order 10 tICs was too small as in nine subjects all 10 tICs were excluded from the analysis due to excessive amount of physiological noise, motion or other artefacts in the signals. In model order 30, roughly 10 tICs passed our exclusion criteria. Model order 50 tICA was able to separate more targeted VLFF signal sources relative to model order that were not excluded. Illustration of the number of excluded components in the model orders 10, 30 and 50 in shown in Supplementary Figure 2. On average in model order 50 tICA, 29 (± 4 std) tICs in DMN_{vmpf} and 27 (± 4) tICs in DMN_{pcc} of a single subject were excluded based on our exclusion criteria. Our signal identification and exclusion criteria claimed that in 50 tICA, DMN_{vmpf} component had significant amount of respiratory activity in 7 tICs (± 2), cardiac in 4 (± 2) tICs, helium in 5 (± 2) tICs, warming in 3 (± 1) tICs and motion in 20 (± 5) tICs. Whereas, DMN_{pcc} component had significant amount of respiratory activity in 6 (± 2) tICs, cardiac in 6 (± 2) tICs, helium in 6 (± 2) tICs, warming in 3 (± 1) tICs and motion in 17 (± 5) tICs. It is noteworthy that even after 99.5 % coverage of signal variance the tICs have contributions from physiological pulsations, motion and system artifacts in > 50 % of IC's. Multiple independent physiological signal sources to be observed were caused by temporal phase fluctuations (see Figure 4), i.e. all physiological components had difference phase even within the same RSN node.

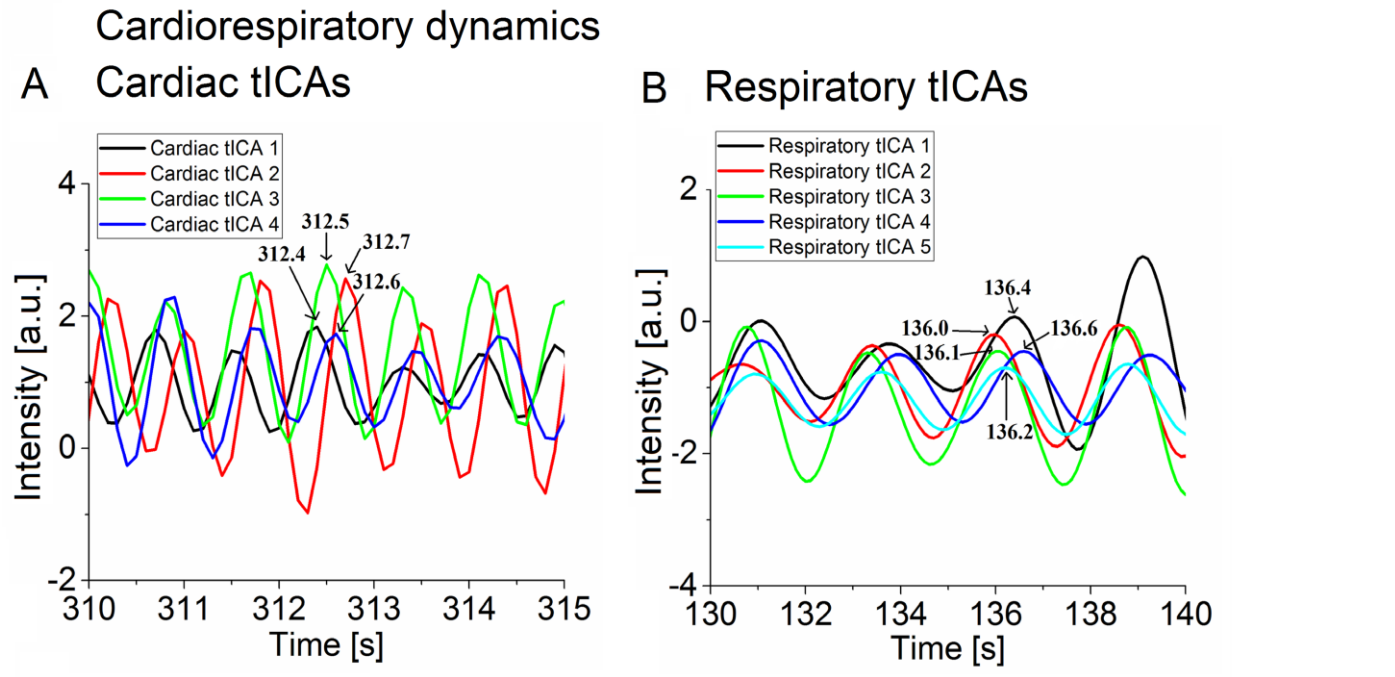

Figure 4. *Illustration of phase shift differences in physiological tIC signals. The signals are enlarged sections of time signals of an individual subject who had 4 cardiac tICs and 5 respiratory tICs identified in DMNvmpf 50 tICA calculation. Notably, all of these physiological signals had a different phase within the spatial IC.*

3.3 Defining statistically significant correlation coefficients and lag values

Statistical significance of the correlation coefficients and lag values were validated by creating histograms from all denoised tICA pair correlation and lag values of 25 subjects (see Figure 5A). The data group consisted of 11 291 data values with mean correlation coefficient of 0.00 and standard deviation of 0.17. Therefore, the threshold of mean ± 3 std ($\mu \pm 3\ \sigma$) was 0.51, indicating that 99.7 % of the correlation coefficients lie within ± 0.51 value range. The mean lag value (see Figure 5B) over all subjects was 0.0 s with standard deviation of 4.0 s.

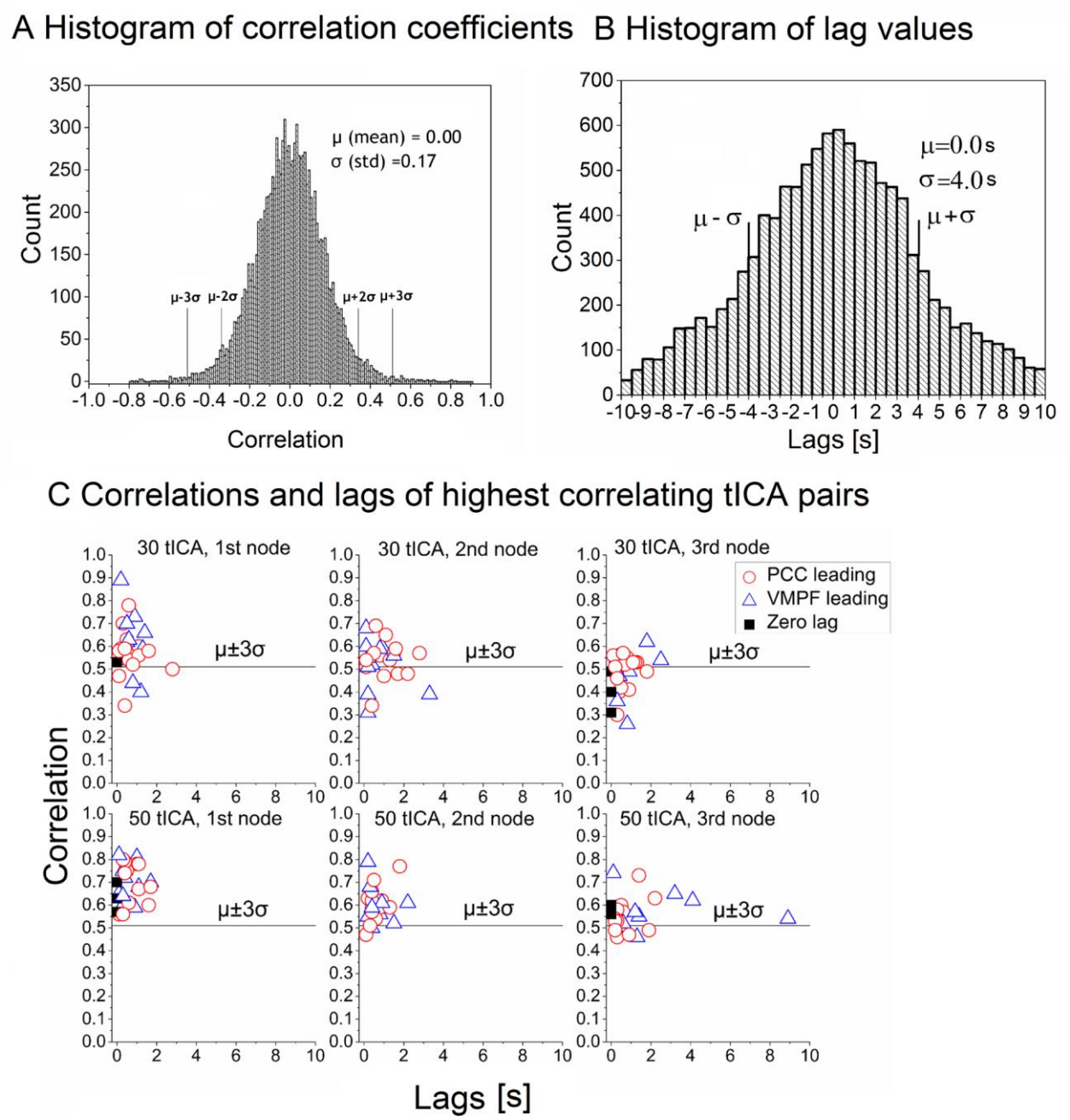

Figure 5. A) *A Histogram of correlation coefficients (between all denoised tICA pairs of all subjects). μ ± 2σ indicates that 95.5 % of the values lie within that range whereas 99.7 % of the values lie within μ ± 2σ range.* ***B)*** *A histogram lag values (between all denoised tICA pairs of all subjects), with the mean lag of 0.0 s and standard deviation of 4.0 s.* ***C)*** *Correlation versus time lags scatterplots of three first nodes in the model order 30 and 50 tICA. The directionality of the leading DMN component is marked by triangle and circle symbols. Correlation values are absolute values. The line of μ ± 3σ indicates the threshold of statistical significance validated in Figure 5A.*

3.4. Cross-individual variability

Cross-individual variability was measured by calculating the lag values between all denoised tICA pairs for all subjects. The null distributions of lag values for all subjects are presented in Figure 6. The results show that the mean lag varies between -0.3…0.5 s and standard deviation vary between 3.6…4.5 s over subjects.

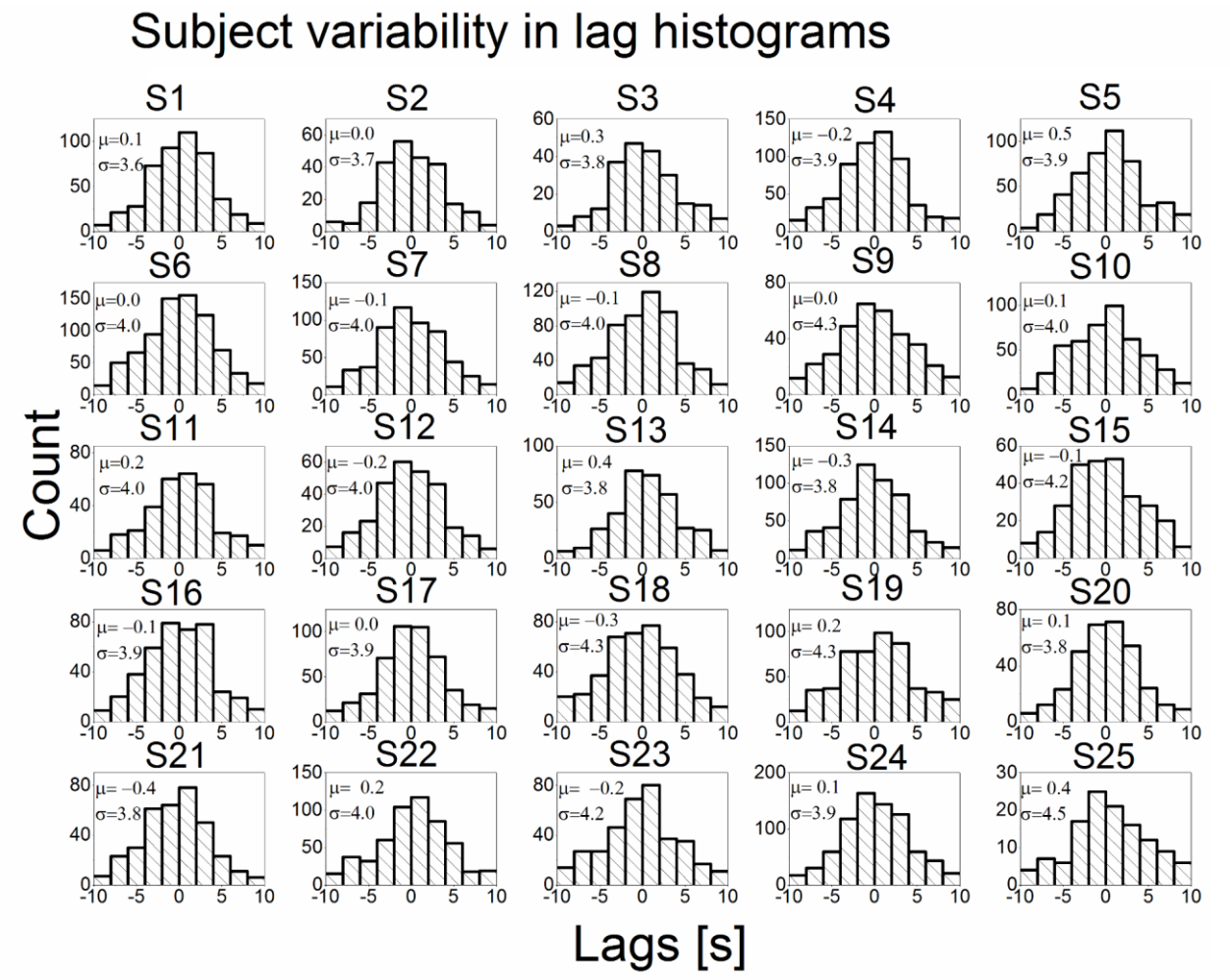

Figure 6. *Subject variability in lag histograms (whole time window). The mean lag over subjects varies between -0.3…0.5s with standard deviation of 3.6...4.5.*

3.5 Continuous and dynamic connectivity

Model order 30 vs 50 tICA connectivity lag estimates of three highest correlating tIC pairs are illustrated in Figure 5C. Lag estimates were not calculated for model order 10 tICA, as only 16 of the 25 subjects had connectivity signal pairs available after exclusion. In each of the nodes, model order 50 tICA showed higher mean absolute correlation values than model order 30 tICA (1st node: 0.69 vs 0.59, 2nd node: 0.60

vs 0.53 and 3rd node: 0.56 vs 0.47). The mean absolute correlation values decreased in both model order of 30 and 50 tICA, as a function of increasing node order. In the first node of model order 50 tICA, each subject had correlation value > 0.55. Moreover, the highest correlating connectivity pairs of all 25 subjects in 50 tICA exceeded the correlation coefficient threshold of 0.51 ($\mu \pm 3\ \sigma$), indicating a probability of 99.7 % to be statistically significant results. Based on the results, the first node of model order 50 tICA was chosen for further analysis.

The mean absolute connectivity time lag was 0.6 s (± 0.5) and mean absolute correlation was 0.69 (± 0.08) in the first node of model order 50 tICA. The directional connectivity between the DMN areas' varied as DMN_{vmpf} preceded DMN_{pcc} in 10 and DMN_{pcc} preceded in 12 cases. Three subjects had a zero lag. Those subjects who had DMN_{vmpf} as preceding component, the mean time lag was 0.6 s (± 0.5) and mean absolute correlation 0.70 (± 0.08). Furthermore, when taking account only the subject results of DMN_{pcc} as preceding component, mean time lag was 0.8 s (± 0.5) and mean absolute correlation 0.70 (± 0.09). Notably > 80 % of the high correlating signal pairs had an elevated activity event peaking in the signal, c.f. Figure 2.

In dynamic connectivity analytics, the correlation coefficient in different time windows was 0.62 ± 0.08. Maximum correlation was on average 0.82 ± 0.07 with a lag of 0.8 s ± 0.7. Subsequent changes in directionality were detected in 1.44 ± 0.9 times of 5 (28.8%) possible number direction changes. The null distributions of correlation coefficients and lag values for each time window are presented in Figure 7, showing marginal sampling variability over time windows. In all time windows, μ=0.00 and σ=0.25 in correlation coefficients, μ=-0.1…0.0 s and σ=4.1…4.2 s in lag values. Detailed dynamic connectivity results of all individual subjects are listed in Supplementary Table I. In 23 of the 25 subjects the mean correlation of all dynamic windows exceeds the $\mu \pm 2$ (± 0.50). Two subjects whose mean correlation (0.47 & 0.45) didn't exceed the $\mu \pm 2$ had still significant correlations in some of the dynamic time windows, i.e. highest correlations being 0.77 & 0.91.

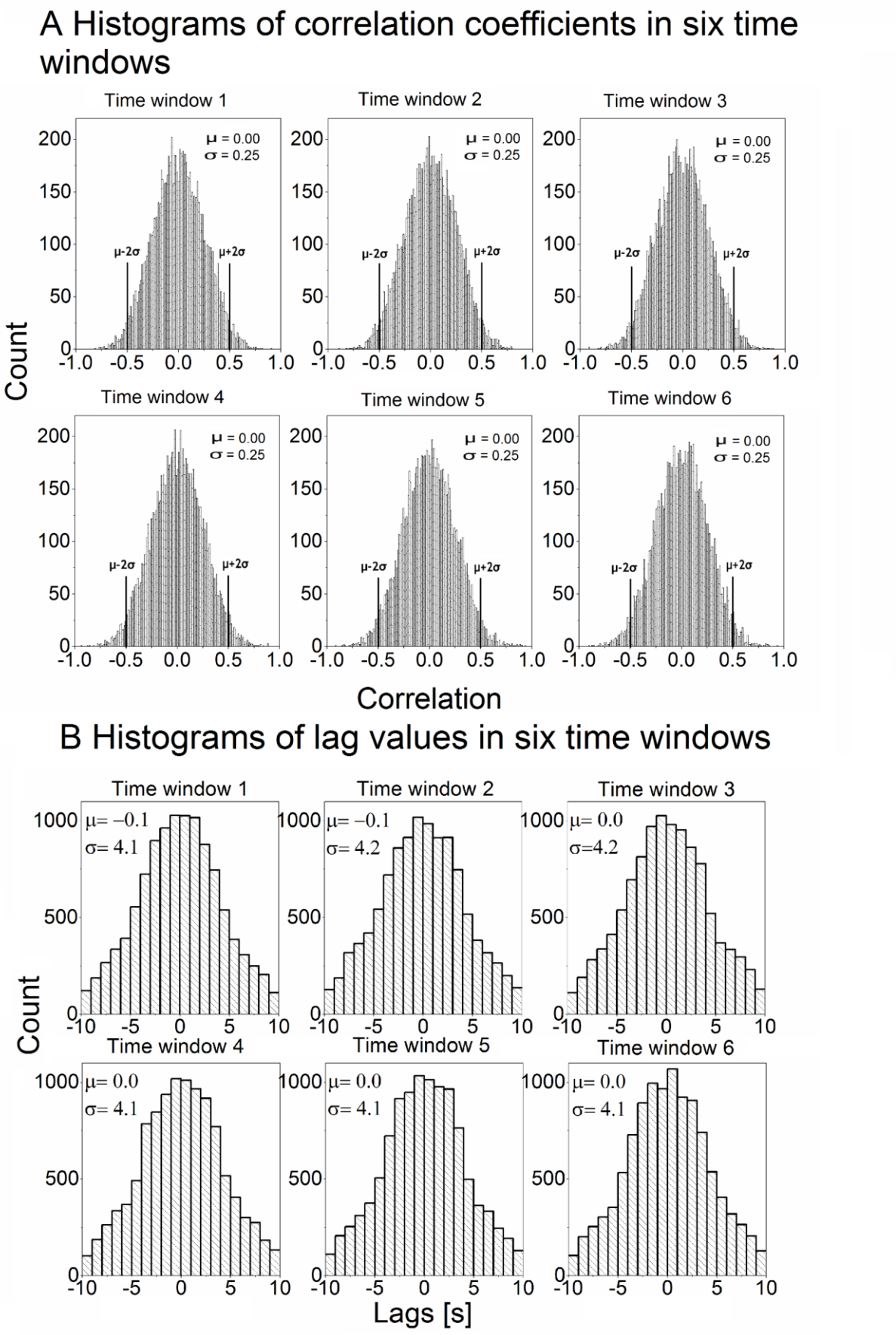
A Histograms of correlation coefficients in six time windows
Time window 1
Time window 2
Time window 3
Time window 4
Time window 5
Time window 6
μ = 0.00
σ = 0.25
μ-2σ
μ+2σ
Count
Correlation
B Histograms of lag values in six time windows
μ= −0.1
σ= 4.1
μ= −0.1
σ= 4.2
μ= 0.0
σ=4.2
μ= 0.0
σ= 4.1
μ= 0.0
σ= 4.1
μ= 0.0
σ= 4.1
Lags [s]

Figure 7. A) *Six histograms of correlation coefficients, presenting six time windows. In all time windows* $\mu=0.00$ *and* $\sigma=0.25$. ***B)*** *The lag value histograms for six time windows. The mean lag is close to zero (-0.1...0.0) in all time windows with almost constant standard deviation (4.1…4.2) over all time windows.*

3.6. Spatial distribution of tICA connectivity

Despite individual spatial variability the most highly correlated tICA VLF signals are confined within the typical DMN nodes. Figure 8 illustrates examples of five subjects showing some variability in the spatial distribution of the three most highly correlated tICA nodes. However there seems to be some spatial overlap between individuals as well in the activity states between DMN areas.

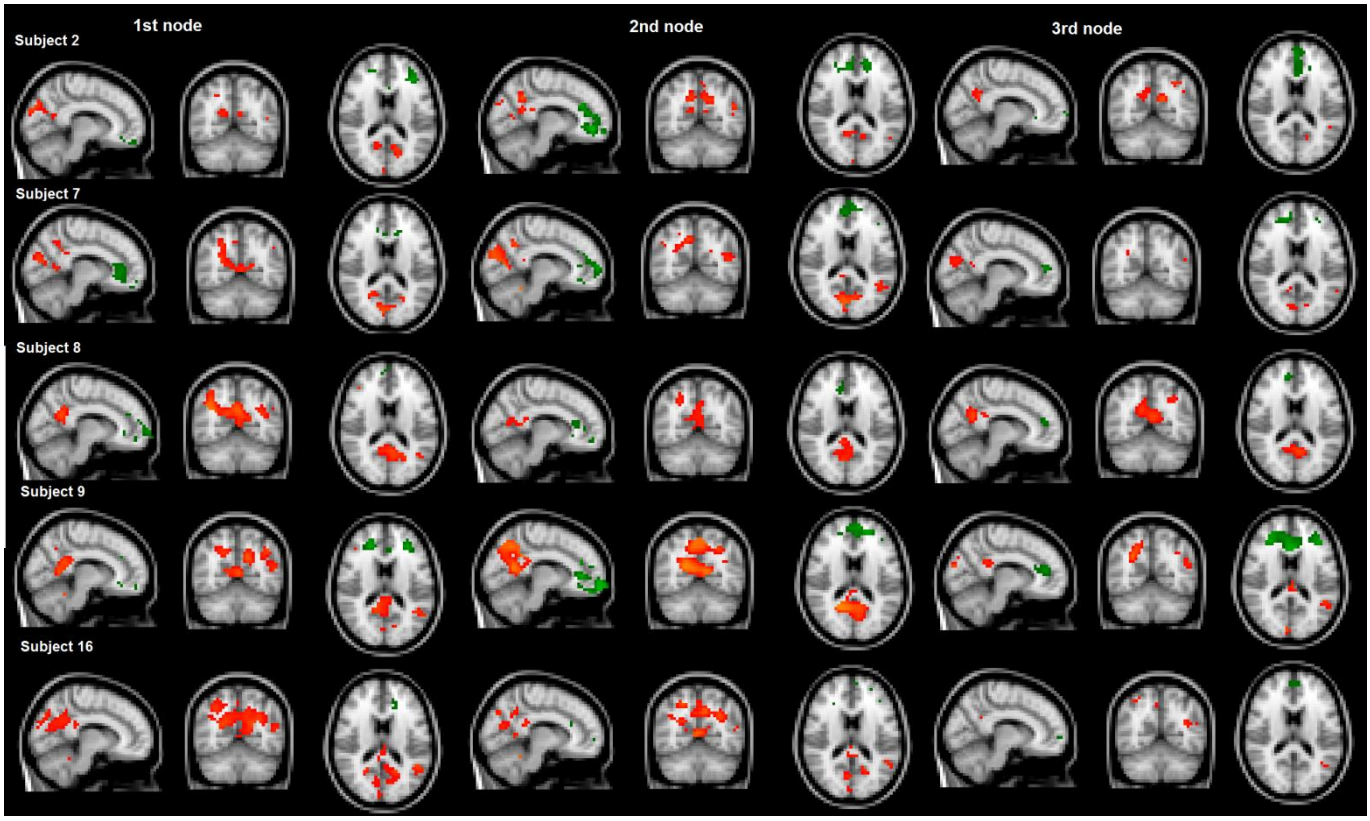

Figure 8. *Spatial distributions of tICA connectivity in five randomly selected subjects. Those voxels whose VLF (0.009-0.1Hz) time signals temporally correlates > 0.3 with tICA are color encoded, .i.e. red color indicating* DMN_{pcc} *and green* DMN_{vmpf} *areas. All images are shown in x=24, y=17, z=22 plane.*

4 DISCUSSION

In this study of MREG data, we extended sICA into a focused tICA in order to obtain robust time domain signals that could enable accurate lag structure estimates between the two opposite ends of DMN. Lag structure estimates were calculated for the highest correlating tICA pairs. Mean time lag of 0.6 s (± 0.5 std) and mean absolute correlation of 0.69 (± 0.08) between the highest correlating tICA pairs of DMN nodes was observed throughout the whole analyzed period. In dynamic 2 min window analysis (of 1200 brain volumes), there was large variability over subjects as in some subjects the lags varied within 1s and in some subjects within 10s time range. Directionality varied between these highly correlating sources an average 28.8% of the possible number of direction changes.

All the de-noised tICs were used to calculate the null-distributions both for expected lag variability over time and over subjects. The null-distributions show highly consistent lag and correlation structure both in continuous and dynamic sliding-window analysis, parallel with prior literature (Mitra et al., 2014; Mitra et al., 2015a). The results support the earlier findings of consistent temporal lags across groups of individuals (Amemiya et al., 2016; Mitra et al., 2014).

Based on the new lag results it seems that is actually very difficult to draw any conclusions that which is the 'leading component' between DMNpcc and DMNvmpf, which support the conclusions by Mitra and co-workers (Mitra et al., 2014) that "each RSN encompasses a range of early and late regions, and no network leads or follows any other network". Rather, lags are equivalently distributed within RSNs". The null-distributions suggest that, when having reasonable amount of samples (nodes), the mean time lag between the DMN nodes is zero, and the probability of having either DMNpcc or DMNvmpf as a 'preceding component' is near equal. Moreover, the standard deviation of time lags in whole time window (Figure 5B) is around 4s, which suggest that all the presented first node lag results lie within the standard deviation, supporting the earlier findings that there is a consistent temporal lag structure across

groups of individuals (Amemiya et al., 2016; Mitra et al., 2014). Therefore, it might be difficult to draw any deep conclusions on average lag results of whole time window since there are only 25 subjects with one lag value. However, these first node results may indicate the largest mutual information change (with highest correlation) which points out that some variability in lag is evident between the highest correlating nodes.

In dynamic analysis, there are lag values exceeding the limits of significance of a null-model meaning that there might be biologically meaningful variation in this measure. Notable, in some subjects the lags seem to have only minor variations (< 1.0 s) over all measured time windows while some subjects there is large variation in the scale of 10 s. It would be interesting to further explore whether this temporal long time lag could mean that there is some strong functional connection between some other RSNs while there is less connectivity within DMN nodes. However, in this study, we have explored the same tICA pair (highest correlating in whole time window) over all time windows. Therefore, the highest connectivity tICA pair can potentially differ dynamically giving much shorter time lag.

Recently, there has been a concern that dynamic BOLD correlations during resting-state could be largely explained by sampling variability, head motion and drowsiness (Laumann et al., 2016). In this study, however, the null-distributions of all time windows suggest that the results in this study do not likely arise from sapling sampling variability since the lag structure shows consistent patterns and lag measures over all time windows. Secondly, in this study the head motion plays very minimal role on dynamics due to the strict motion exclusion criteria we have applied to the data. Thirdly, the drowsiness, could in theory infer some dynamics. However, we have used the initial 7 mins scan for the analysis. Therefore the subjects should be fairly vigilant, since the vigilance is always checked (orally) between each scan.

Mitra and co-workers extrapolated a highly reproducible lags on the order of ~1s by application of parabolic interpolation of 3 s TR resting state BOLD data (Mitra et al., 2015a), which matched relatively well to lag values of highest correlating tICA pairs obtained with critically sampled data of this study.

Furthermore, Mitra et al., demonstrated multiple lag threads, some of which can be physiological like hemodynamic and some neurophysiological in origin (Mitra et al., 2015a). First of all many tICA sources are affected by cardiorespiratory pulses that have different phases since the pulses move in the brain. Furthermore, we were also able to depict several other connectivity tICs that were not noise sources, which also support the finding of multiple lag threads in the data, even within DMN key sub-network nodes.

The VLFF signal in the RSN's including the DMN can be thought of as a series of repeating signal intensity peaks similar to neuronal avalanches (Liu & Duyn 2013, Palva et al., 2014). It has been shown that the DMN splitting into several spatially independent signal sources follows individual paths of these neuronal avalanches (Abou Elseoud et al., 2011; Kiviniemi et al., 2009; Rajna et al., 2015). A preliminary finding in animal experiments supports this, as the white matter DMN connections are anatomically patchy (Heilbronner SR, 2014). Interestingly the spatial distributions of the highest connectivity tIC nodes show very similar anatomical moment to moment variability most likely stemming from segregated and unique sources of connectivity (Kiviniemi et al., 2011).

Also as ICA has a tendency towards sparseness, the tICA may select a signal source based on strong individual events in the data (Daubechies et al., 2009). The finding of strong signal peaks during high connectivity supports the idea of neuronal avalanches driving the dynamic connectivity; individual brain activity avalanches present strong connectivity patterns that sum up into a VLFF signal pattern when averaged over a longer period in time (Liu and Duyn, 2013; Palva et al., 2013; Rajna et al., 2015). It remains to be seen whether these temporally subsequent avalanches form the statistical independence that ICA picks up.

We believe that the lag variations even within sources with highest connectivity across subjects can be reflecting previously described dynamic rather than the stable nature of functional connectivity (Chang and Glover, 2010; Hutchison et al., 2013; Kiviniemi et al., 2011). As most changes in neural processing

occur in the millisecond range, our current MREG data takes 20 more accurate step towards that temporal resolution. Due to the increased temporal accuracy, we are also now more sensitive to moment to moment changes also in directionality.

In order to maximize the probability of analyzing functional connectivity within the DMN we focused solely on highest connectivity signal pairs. Notably > 80 % of the high correlating DMN signal pairs had an elevated activity event peaking in the signal (see Figure 3). We believe that these elevated activities represent neuronal avalanches (Liu et al., 2013; Palva et al., 2013; Rajna et al., 2015) and as sparse events the avalanches dominate the connectivity structure. Our strict exclusion criterion minimizes the probability that those elevated signal peaks are not caused by physiological noise, motion or system artefacts. However, the dynamic 4D mapping of individual neuronal avalanches might reveal a more accurate description of the lag structure and especially dynamics in directionality, which we intend to investigate in the future (Liu and Duyn, 2013; Palva et al., 2013; Rajna et al., 2015).

Future work

Since the brain pulsates strongly, it is mandatory to separate the physiological pulsations from neuronal activity (Birn at al., 2006; Kiviniemi et al., 2015). In this study we show that tICA, even with signals focused on DMN by sICA pre-processing, tICs are still affected by noise sources like motion and pulsations to varying extent. This implies that the physiological pulsations are not temporally independent nor sparse but rather continuous and omnipresent (Kiviniemi et al., 2015). In critically sampled data, the same physiological pulses extend over the brain in repeating waves. This implies that in de facto each neighboring voxel has a temporally phase shifted signal in cardiorespiratory as well as very low frequencies that may also interference in unexpected ways within the same RSN. These multiple phase representations of signal sources seem to become detected as separate temporal IC. Despite the idea of superior performance of tICA in the detection of neuronal events, the physiological pulsations driving the brain glymphatic system may actually mask the neuronal events. This needs to be countered with higher

model order of tICs, which complicates analysis. However advanced filtering prior to tICA needs to be analyzed in the future.

It would be interesting to know how tICA would improve, if the continuous noise sources such as pulsations would be removed a priori using sICA approaches. Fully automatic *spatial* noise detection algorithm, such as FIX "FMRIB's ICA based X-noisifier"), could in theory offer a valuable pre-processing step before stICA procedure for denoising fMRI data via accurate classification of ICA components (Griffanti et al., 2014; Salimi-Khorshidi et al., 2014). We aim to automate RSN tICs detection and explore how the connectivity dynamics are affecting the lag thread structure and directionality with a matrix approach. The identification of disruptions in the lag structure of the brain can be useful for clinical applications such as studying patients with variable neuronal and psychiatric brain diseases. Recent work by Mitra and co-workers has already shown that lag-structure of intrinsic activity is focally altered in high functioning adults with autism (Mitra et al., 2015b).

5 CONCLUSIONS

Combined spatiotemporal ICA (stICA) of critically sampled MREG data separated accurately the VLF signals from physiological, motion and other artefact signal sources which further enabled accurate lag structure estimates between DMN nodes. The null model distributions show highly consistent correlation and lag structure between DMN nodes both in continuous and dynamic analysis. The mean time lag of a null model between DMN nodes was 0.0 s and thus the probability of having either DMNpcc or DMNvmpf as a preceding component is near equal. All the lag values of highest correlating tICA pairs over subjects lie within the standard deviation range of a null-model in whole time window analysis, supporting the earlier findings that there is a consistent temporal lag structure across groups of individuals. However, in dynamic analysis, there are lag values exceeding the limits of significance of a null-model meaning that there might be biologically meaningful variation in this measure. Furthermore, most of the signal sources with highest tICA connectivity pairs show a momentary activity peaks in the signals that dominate the connectivity structure over the measured period, suggesting that individual avalanches may play an important role in defining dynamic independence in resting state connectivity within networks.

ACKNOWLEDGEMENTS

This study was financially supported by Academy of Finland Grant 275352 (MREG Analysis of Neuronal Avalanches), JAES grant and MRC Oulu grant. Additional thanks to Finnish Epilepsy Association (FEA) and Walter Ahlström foundation who supported this research by personal grant.

REFERENCES

Abou Elseoud, A., Littow, H., Remes, J., Starck, T., Nikkinen, J., Nissila, J., Timonen, M., Tervonen, O., Kiviniemi, V., 2011. Group-ICA model order highlights patterns of functional brain connectivity. Front. Syst. Neurosci. 5, 37.

Amemiya, S., Takao, H., Hanaoka, S., Ohtomo, K., 2016. Global and structured waves of rs-fMRI signal identified as putative propagation of spontaneous neural activity. Neuroimage. 133, 331-340.

Assländer, J., Zahneisen, B., Hugger, T., Reisert, M., Lee, H., LeVan, P., Hennig, J., 2013. Single shot whole brain imaging using spherical stack of spirals trajectories. Neuroimage. 73, 59-70.

Barbieri, R., Shimono, M., 2012. Criticality in large-scale brain fMRI dynamics unveiled by a novel point process analysis. Networking of Psychophysics, Psychology and Neurophysiology, 61.

Beall, E.B., Lowe, M.J., 2014. SimPACE: Generating simulated motion corrupted BOLD data with synthetic-navigated acquisition for the development and evaluation of SLOMOCO: A new, highly effective slicewise motion correction. Neuroimage. 101, 21-34.

Beckmann, C.F., DeLuca, M., Devlin, J.T., Smith, S.M., 2005. Investigations into resting-state connectivity using independent component analysis. Philos. Trans. R. Soc. Lond. B. Biol. Sci. 360, 1001-1013.

Birn, R.M., Diamond, J.B., Smith, M.A., Bandettini, P.A., 2006. Separating respiratory-variation-related fluctuations from neuronal-activity-related fluctuations in fMRI. Neuroimage. 31, 1536-1548.

Biswal, B., Yetkin, F.Z., Haughton, V.M., Hyde, J.S., 1995. Functional connectivity in the motor cortex of resting human brain using echo-planar MRI. Magnetic Resonance in Medicine. 34, 537-541.

Biswal, B.B., Ulmer, J.L., 1999. Blind source separation of multiple signal sources of fMRI data sets using independent component analysis. J. Comput. Assist. Tomogr. 23, 265-271.

Boubela, R.N., Kalcher, K., Huf, W., Kronnerwetter, C., Filzmoser, P., Moser, E., 2013. Beyond noise: Using temporal ICA to extract meaningful information from high-frequency fMRI signal fluctuations during rest. Frontiers in Human Neuroscience. 7.

Boyacioglu, R., Beckmann, C., Barth, M., 2013. An investigation of RSN frequency spectra using ultra-fast generalized inverse imaging (GIN). Front Hum Neurosci. 7, 156.

Boyacioğlu, R., Barth, M., 2013. Generalized iNverse imaging (GIN): Ultrafast fMRI with physiological noise correction. Magnetic Resonance in Medicine. 70, 962-971.

Calhoun, V., Adali, T., Pearlson, G., Pekar, J., 2001. A method for making group inferences from functional MRI data using independent component analysis. Hum. Brain Mapp. 14, 140-151.

Calhoun, V., Adali, T., Stevens, M., Kiehl, K., Pekar, J., 2005. Semi-blind ICA of fMRI: A method for utilizing hypothesis-derived time courses in a spatial ICA analysis. Neuroimage. 25, 527-538.

Chang, C., Glover, G.H., 2010. Time–frequency dynamics of resting-state brain connectivity measured with fMRI. Neuroimage. 50, 81-98.

Chiew, M., Graedel, N.N., McNab, J.A., Smith, S.M., Miller, K.L., 2016. Accelerating functional MRI using fixed-rank approximations and radial-cartesian sampling. Magnetic Resonance in Medicine.
Chiew, M., Smith, S.M., Koopmans, P.J., Graedel, N.N., Blumensath, T., Miller, K.L., 2015. K-t FASTER: Acceleration of functional MRI data acquisition using low rank constraints. Magnetic Resonance in Medicine. 74, 353-364.
Damoiseaux, J.S., Rombouts, S.A., Barkhof, F., Scheltens, P., Stam, C.J., Smith, S.M., Beckmann, C.F., 2006. Consistent resting-state networks across healthy subjects. Proc. Natl. Acad. Sci. U. S. A. 103, 13848-13853.
Daubechies, I., Roussos, E., Takerkart, S., Benharrosh, M., Golden, C., D'Ardenne, K., Richter, W., Cohen, J.D., Haxby, J., 2009. Independent component analysis for brain fMRI does not select for independence. Proc. Natl. Acad. Sci. U. S. A. 106, 10415-10422.
Esposito, F., Scarabino, T., Hyvarinen, A., Himberg, J., Formisano, E., Comani, S., Tedeschi, G., Goebel, R., Seifritz, E., Di Salle, F., 2005. Independent component analysis of fMRI group studies by self-organizing clustering. Neuroimage. 25, 193-205.
Greicius, M.D., Srivastava, G., Reiss, A.L., Menon, V., 2004. Default-mode network activity distinguishes alzheimer's disease from healthy aging: Evidence from functional MRI. Proc. Natl. Acad. Sci. U. S. A. 101, 4637-4642.
Griffanti, L., Salimi-Khorshidi, G., Beckmann, C.F., Auerbach, E.J., Douaud, G., Sexton, C.E., Zsoldos, E., Ebmeier, K.P., Filippini, N., Mackay, C.E., 2014. ICA-based artefact removal and accelerated fMRI acquisition for improved resting state network imaging. Neuroimage. 95, 232-247.
Heilbronner SR, H.S., 2014. Anatomical connections subserving the default mode network. Society for Neuroscience, Annual Meeting. 563.21.
Hugger, T., Zahneisen, B., LeVan, P., Lee, K.J., Lee, H., Zaitsev, M., Hennig, J., 2011. Fast undersampled functional magnetic resonance imaging using nonlinear regularized parallel image reconstruction. PloS One. 6, e28822.
Hutchison, R.M., Womelsdorf, T., Gati, J.S., Everling, S., Menon, R.S., 2013. Resting-state networks show dynamic functional connectivity in awake humans and anesthetized macaques. Hum. Brain Mapp. 34, 2154-2177.
Hyvärinen, A., Oja, E., 1997. A fast fixed-point algorithm for independent component analysis. Neural Comput. 9, 1483-1492.
Jafri, M.J., Pearlson, G.D., Stevens, M., Calhoun, V.D., 2008. A method for functional network connectivity among spatially independent resting-state components in schizophrenia. Neuroimage. 39, 1666-1681.
Jenkinson, M., Beckmann, C.F., Behrens, T.E., Woolrich, M.W., Smith, S.M., 2012. Fsl. Neuroimage. 62, 782-790.
Kiviniemi, V., Ruohonen, J., Tervonen, O., 2005. Separation of physiological very low frequency fluctuation from aliasing by switched sampling interval fMRI scans. Magn. Reson. Imaging. 23, 41-46.
Kiviniemi, V., Kantola, J., Jauhiainen, J., Hyvärinen, A., Tervonen, O., 2003. Independent component analysis of nondeterministic fMRI signal sources. Neuroimage. 19, 253-260.
Kiviniemi, V., Vire, T., Remes, J., Elseoud, A.A., Starck, T., Tervonen, O., Nikkinen, J., 2011. A sliding time-window ICA reveals spatial variability of the default mode network in time. Brain Connectivity. 1, 339-347.

Kiviniemi, V., Starck, T., Remes, J., Long, X., Nikkinen, J., Haapea, M., Veijola, J., Moilanen, I., Isohanni, M., Zang, Y., 2009. Functional segmentation of the brain cortex using high model order group PICA. Hum. Brain Mapp. 30, 3865-3886.
Kiviniemi, V., Wang, X., Korhonen, V., Keinanen, T., Tuovinen, T., Autio, J., LeVan, P., Keilholz, S., Zang, Y.F., Hennig, J., Nedergaard, M., 2015. Ultra-fast magnetic resonance encephalography of physiological brain activity - glymphatic pulsation mechanisms? J. Cereb. Blood Flow Metab.
Korhonen, V., Hiltunen, T., Myllylä, T., Wang, X., Kantola, J., Nikkinen, J., Zang, Y., LeVan, P., Kiviniemi, V., 2014. Synchronous multiscale neuroimaging environment for critically sampled physiological analysis of brain function: Hepta-scan concept. Brain Connectivity. 4, 677-689.
Laumann, T.O., Snyder, A.Z., Mitra, A., Gordon, E.M., Gratton, C., Adeyemo, B., Gilmore, A.W., Nelson, S.M., Berg, J.J., Greene, D.J., McCarthy, J.E., Tagliazucchi, E., Laufs, H., Schlaggar, B.L., Dosenbach, N.U., Petersen, S.E., 2016. On the stability of BOLD fMRI correlations. Cereb. Cortex.
Lee, H., Zahneisen, B., Hugger, T., LeVan, P., Hennig, J., 2013. Tracking dynamic resting-state networks at higher frequencies using MR-encephalography. Neuroimage. 65, 216-222.
Leonardi, N., Van De Ville, D., 2015. On spurious and real fluctuations of dynamic functional connectivity during rest. Neuroimage. 104, 430-436.
Lin, F., Ahveninen, J., Raij, T., Witzel, T., Chu, Y., Jääskeläinen, I.P., Tsai, K.W., Kuo, W., Belliveau, J.W., 2014. Increasing fMRI sampling rate improves granger causality estimates. PloS One. 9, e100319.
Lin, F., Witzel, T., Raij, T., Ahveninen, J., Tsai, K.W., Chu, Y., Chang, W., Nummenmaa, A., Polimeni, J.R., Kuo, W., 2013. fMRI hemodynamics accurately reflects neuronal timing in the human brain measured by MEG. Neuroimage. 78, 372-384.
Liu, X., Duyn, J.H., 2013. Time-varying functional network information extracted from brief instances of spontaneous brain activity. Proceedings of the National Academy of Sciences. 110, 4392-4397.
Liu, X., Chang, C., Duyn, J.H., 2013. Decomposition of spontaneous brain activity into distinct fMRI co-activation patterns. Front. Syst. Neurosci. 7, 101.
Majeed, W., Magnuson, M., Hasenkamp, W., Schwarb, H., Schumacher, E.H., Barsalou, L., Keilholz, S.D., 2011. Spatiotemporal dynamics of low frequency BOLD fluctuations in rats and humans. Neuroimage. 54, 1140-1150.
Matsui, T., Murakami, T., Ohki, K., 2016. Transient neuronal coactivations embedded in globally propagating waves underlie resting-state functional connectivity. Proc. Natl. Acad. Sci. U. S. A. 113, 6556-6561.
McKeown, M.J., Jung, T.P., Makeig, S., Brown, G., Kindermann, S.S., Lee, T.W., Sejnowski, T.J., 1998. Spatially independent activity patterns in functional MRI data during the stroop color-naming task. Proc. Natl. Acad. Sci. U. S. A. 95, 803-810.
Mitra, A., Snyder, A.Z., Blazey, T., Raichle, M.E., 2015a. Lag threads organize the brain's intrinsic activity. Proceedings of the National Academy of Sciences. 112, E2235-E2244.
Mitra, A., Snyder, A.Z., Hacker, C.D., Pahwa, M., Tagliazucchi, E., Laufs, H., Leuthardt, E.C., Raichle, M.E., 2016. Human cortical–hippocampal dialogue in wake and slow-wave sleep. Proceedings of the National Academy of Sciences, 201607289.

Mitra, A., Snyder, A.Z., Hacker, C.D., Raichle, M.E., 2014. Lag structure in resting-state fMRI. J. Neurophysiol. 111, 2374-2391.
Mitra, A., Snyder, A.Z., Constantino, J.N., Raichle, M.E., 2015b. The lag structure of intrinsic activity is focally altered in high functioning adults with autism. Cereb. Cortex.
Narsude, M., Gallichan, D., Van Der Zwaag, W., Gruetter, R., Marques, J.P., 2015. Three-dimensional echo planar imaging with controlled aliasing: A sequence for high temporal resolution functional MRI. Magnetic Resonance in Medicine.
Palva, J.M., Zhigalov, A., Hirvonen, J., Korhonen, O., Linkenkaer-Hansen, K., Palva, S., 2013. Neuronal long-range temporal correlations and avalanche dynamics are correlated with behavioral scaling laws. Proc. Natl. Acad. Sci. U. S. A. 110, 3585-3590.
Posse, S., Ackley, E., Mutihac, R., Zhang, T., Hummatov, R., Akhtari, M., Chohan, M., Fisch, B., Yonas, H., 2013. High-speed real-time resting-state fMRI using multi-slab echo-volumar imaging. Frontiers in Human Neuroscience. 7.
Rajna, Z., Kananen, J., Keskinarkaus, A., Seppänen, T., Kiviniemi, V., 2015. Detection of short-term activity avalanches in human brain default mode network with ultrafast MR encephalography. Frontiers in Human Neuroscience. 9.
Salimi-Khorshidi, G., Douaud, G., Beckmann, C.F., Glasser, M.F., Griffanti, L., Smith, S.M., 2014. Automatic denoising of functional MRI data: Combining independent component analysis and hierarchical fusion of classifiers. Neuroimage. 90, 449-468.
Shakil, S., Keilholz, S.D., Lee, C., 2015. On frequency dependencies of sliding window correlation. , 363-368.
Smith, S.M., Miller, K.L., Salimi-Khorshidi, G., Webster, M., Beckmann, C.F., Nichols, T.E., Ramsey, J.D., Woolrich, M.W., 2011. Network modelling methods for FMRI. Neuroimage. 54, 875-891.
Smith, S.M., Miller, K.L., Moeller, S., Xu, J., Auerbach, E.J., Woolrich, M.W., Beckmann, C.F., Jenkinson, M., Andersson, J., Glasser, M.F., Van Essen, D.C., Feinberg, D.A., Yacoub, E.S., Ugurbil, K., 2012. Temporally-independent functional modes of spontaneous brain activity. Proc. Natl. Acad. Sci. U. S. A. 109, 3131-3136.
Tagliazucchi, E., Balenzuela, P., Fraiman, D., Montoya, P., Chialvo, D.R., 2011. Spontaneous BOLD event triggered averages for estimating functional connectivity at resting state. Neurosci. Lett. 488, 158-163.
Thompson, G.J., Pan, W., Magnuson, M.E., Jaeger, D., Keilholz, S.D., 2014. Quasi-periodic patterns (QPP): Large-scale dynamics in resting state fMRI that correlate with local infraslow electrical activity. Neuroimage. 84, 1018-1031.
Thompson, G.J., Pan, W.J., Keilholz, S.D., 2015. Different dynamic resting state fMRI patterns are linked to different frequencies of neural activity. J. Neurophysiol. 114, 114-124.
van de Ven, Vincent G, Formisano, E., Prvulovic, D., Roeder, C.H., Linden, D.E., 2004. Functional connectivity as revealed by spatial independent component analysis of fMRI measurements during rest. Hum. Brain Mapp. 22, 165-178.
Zahneisen, B., Hugger, T., Lee, K.J., LeVan, P., Reisert, M., Lee, H., Assländer, J., Zaitsev, M., Hennig, J., 2012. Single shot concentric shells trajectories for ultra fast fMRI. Magnetic Resonance in Medicine. 68, 484-494.

Supplements

Supplement Figure 1

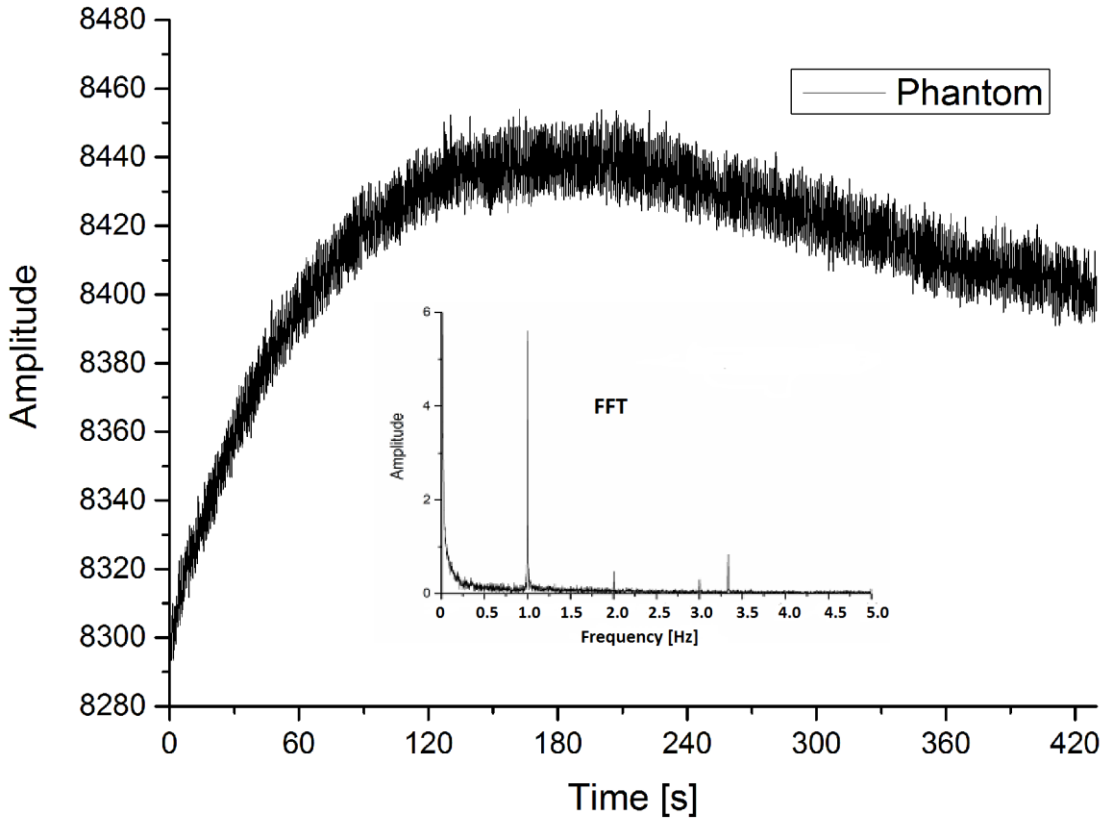

Figure presents the signal warming behavior verified by phantom test using the same MREG imaging setup. The warming causes the signal amplitude to rise strongly during the first 120 s before it reaches its maximum. FFT shows that significant amount of 1 Hz (Skyra helium pump) noise is included in the warming curve.

Supplement Figure 2

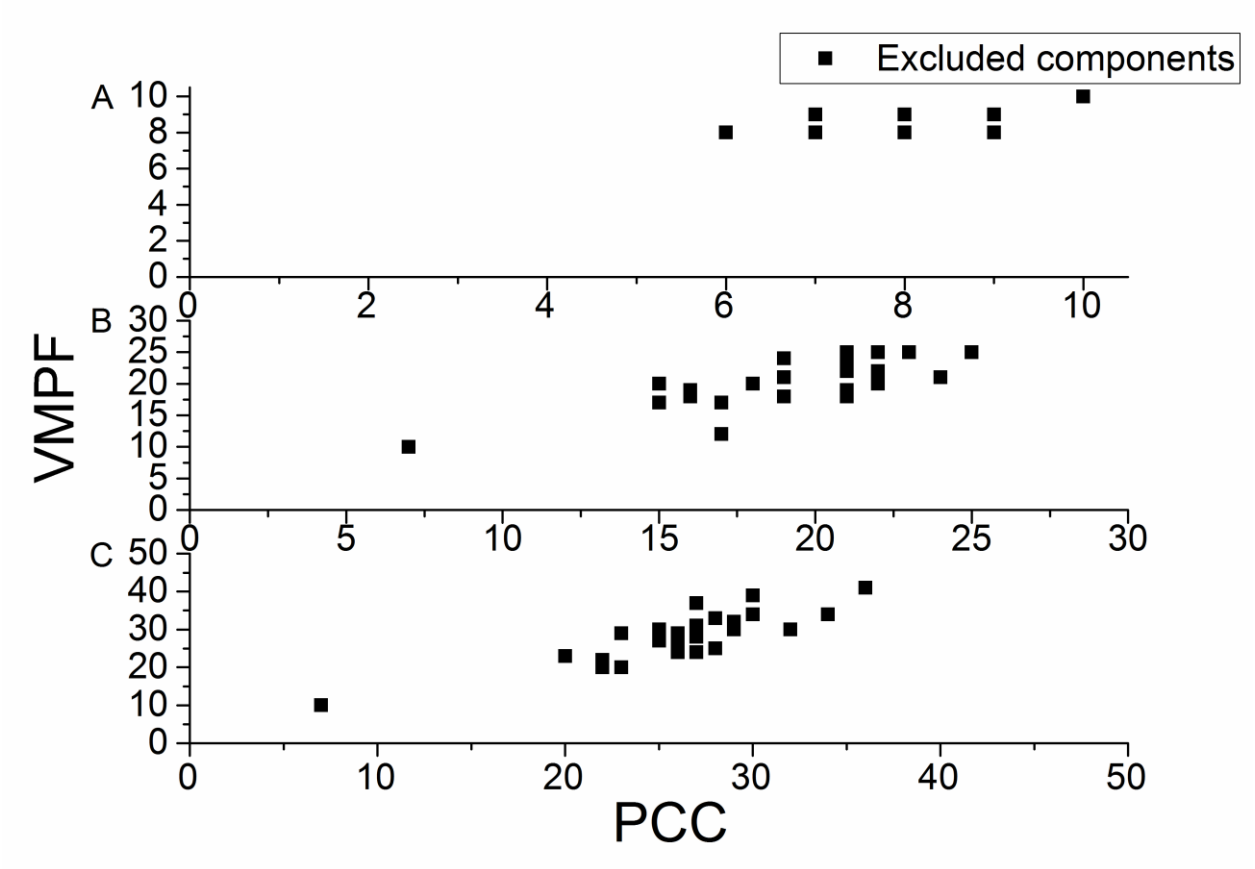

Illustration of excluded temporal ICA components in each of the 25 subjects. Panel (A) shows 10 tICA, (B) 30 tICA and (C) 50 tICA. X-axis indicates the number of excluded tICAs in DMN_{pcc} *and y-axis in* DMN_{vmpf}*. Next, the excluded component pairs that included more than 1 subject are listed. In 10 tICA; 9 subjects (10 VMPF excluded, 10 PCC excluded), 7 subjects (9,9), 2 subjects (8,9), 2 subjects (8,8), 2 subjects (9,7). In 30 tICA; 2 subjects (25,23), In 50 tICA; 2 subjects (21,19), 2 subjects (30,32).*

Supplementary Table I. *Dynamic connectivity results of each of the individual subjects.*

50 tICA	Dynamics (6 time windows, 2 mins long, 1 min overlap) 1 2 3 4 5 6							
subject	corr lag	corr lag	corr lag	corr lag	corr lag	corr lag	mean corr mean lag	corr std lag std
1	-0.74 0.4	-0.68 -0.4	-0.62 -0.4	-0.8 1.4	-0.61 -0.4	-0.42 -5.9	0.65 1.5	0.13 2.2
2	0.51 0.6	0.53 0.3	0.60 -0.8	0.54 -1.6	0.80 -0.6	0.71 -0.4	0.62 0.7	0.12 0.5
3	-0.78 1.9	-0.76 1.7	-0.80 0.1	-0.87 1.1	-0.83 1.4	-0.63 0.8	0.78 1.2	0.08 0.7
4	0.15 2.7	0.67 0.0	0.62 1.2	0.45 -1.6	0.63 -1.1	0.86 -0.5	0.56 1.2	0.24 0.9
5	0.67 0.0	0.69 0.8	0.62 1.0	0.81 0.1	0.81 -0.3	0.59 -0.5	0.70 0.5	0.09 0.4
6	0.68 1.2	0.82 1.3	0.89 0.4	0.89 -0.7	0.65 -0.4	0.5 -1.5	0.74 0.9	0.16 0.5
7	0.60 1.9	0.50 -1.1	0.66 -1.5	0.89 -0.3	0.91 0	0.84 0.5	0.73 0.9	0.17 0.7
8	-0.22 3.8	0.33 -4.0	0.75 0.2	0.77 0.4	0.51 1.6	0.26 2.2	0.47 2.0	0.24 1.6
9	0.70 -1.0	0.43 -0.5	0.69 0.2	0.83 -1.4	0.88 -1.7	0.85 -2.2	0.73 1.2	0.17 0.8
10	-0.32 1.2	-0.46 0.2	-0.71 -0.4	-0.63 0.3	-0.85 0.0	-0.86 0.5	0.64 0.4	0.22 0.4
11	-0.38 -10.0	-0.59 -0.7	-0.56 -3.6	-0.71 -2.9	-0.59 -1.8	-0.78 -0.8	0.60 3.3	0.14 3.5
12	-0.35 1.1	-0.23 1.5	-0.48 0.2	-0.55 -0.2	-0.66 -0.3	-0.74 0.1	0.50 0.6	0.19 0.6
13	0.58 0.4	0.63 -0.3	0.48 -2.8	0.61 1.1	0.58 0.9	0.64 0.1	0.59 0.9	0.06 1.0
14	-0.70 -0.9	-0.54 -0.8	-0.68 0.0	-0.87 -0.3	-0.84 -0.5	-0.39 10.0	0.67 2.1	0.18 3.9
15	0.30 0.9	0.60 -0.7	0.66 -0.8	0.85 2.4	0.77 2.2	0.35 -8.2	0.59 2.5	0.22 2.9
16	0.54 -0.7	0.52 -1.3	0.67 -1.0	0.68 -0.5	0.63 -1.0	0.64 -1.0	0.61 0.9	0.07 0.3
17	-0.64 10.0	0.52 1.0	0.86 1.6	0.77 1.2	0.50 -10	0.45 -0.9	0.62 4.1	0.17 4.6
18	0.91 0.5	0.46 1.4	0.43 1.7	0.27 9.8	0.36 -4.6	0.28 -4.3	0.45 3.7	0.24 3.4
19	-0.45 -10.0	-0.91 0.6	-0.92 0.6	-0.65 -0.5	-0.46 -1.0	-0.35 -10.0	0.62 3.8	0.25 4.8
20	0.39 0.8	0.73 2.1	0.63 1.6	0.75 1.8	0.79 2.1	0.61 1.5	0.65 1.7	0.15 0.5
21	0.75 -0.1	0.63 -0.7	0.57 -0.5	0.61 0.7	0.56 0.3	0.52 0.4	0.61 0.5	0.08 0.2
22	0.46 4.8	-0.27 -9.1	-0.36 -5.3	-0.83 -2.2	-0.87 -1.9	-0.66 -0.1	0.58 3.9	0.25 3.2

23	**-0.33** **-3.0**	**-0.41** **-1.6**	**-0.67** **-0.4**	**-0.58** **-0.1**	**-0.87** **1.4**	**-0.91** **1.6**	**0.63** **1.4**	**0.24** **1.0**
24	**0.66** **-0.1**	**0.62** **-0.1**	**0.63** **-0.7**	**0.45** **-1.3**	**0.72** **0.0**	**0.78** **0.1**	**0.64** **0.4**	**0.11** **0.5**
25	**0.40** **-9.4**	**0.48** **-7.3**	**-0.45** **7.8**	**-0.69** **-1.0**	**-0.76** **-0.7**	**-0.70** **0.0**	**0.58** **4.4**	**0.15** **4.2**

Figure captions

Figure 1. *General workflow of stICA. First, spatial ICA is run to the whole brain volume using FSL MELODIC's 'multi-session temporal concatenation' and two IC components* DMN_{vmpf} *and* DMN_{pcc} *are selected (lef box). The time series of voxels within* DMN_{vmpf} *and* DMN_{pcc} *IC maps that exceed the selected threshold (z>3) are chosen for tICA analysis. Right box presents example tICs of an individual subject.*

Figure 2. A. *Estimation of connectivity time lag. Once the best correlating tICs between two spatial ROIs (here* DMN_{pcc} *and* DMN_{vmpf}*) were selected after strict tICA exclusion criteria, the selected tICs were band pass filtered 0.009-0.1 Hz and then correlated. The other signal was shifted by sample +/- 100 samples, i.e. 10 s and the time lag that gave the strongest correlation was declared as time lag between DMN front and back components. The elevated activity is seen in both tICs.* ***B.*** *Estimation of connectivity dynamics. Connectivity dynamics calculations were applied to the best correlating and BP filtered (0.009-0.1 Hz) tICs in Figure 2A. We formed six time windows of 2 mins length and 1 mins overlap. In each time window the other signal was shifted by sample +/- 100 samples, i.e. 10 s and the time lag that gave the strongest correlation was declared as time lag between DMN front and back components.*

Figure 3. A. *Overview of signal sources of a single subject including time signals and corresponding FFTs is presented in Figure 7. Temporal ICs are named based on our identification and exclusion criteria (see section Identification and exclusion criteria for tICAs) referring to the most prominent feature (cardiac, respiration, helium, warming, motion and VLFF) in tICA. Signals 1 and 2 represent VLFF signals typical to RSN's as they have passed all exclusion criteria.* ***B.*** *Typical cardiac (above) and respiratory (bottom) signals of DMNvmpf calculated with stICA. The cardiac tIC includes a clear M-shape that is seen in the enlarged section (100-120 s) of the signal, presents the aortic closure wedge on the arterial pulse.*

Figure 4. *Illustration of phase shift differences in physiological tIC signals. The signals are enlarged sections of time signals of an individual subject who had 4 cardiac tICs and 5 respiratory tICs identified in DMNvmpf 50 tICA calculation. Notably, all of these physiological signals had a different phase within the spatial IC.*

Figure 5. A) *A Histogram of correlation coefficients (between all denoised tICA pairs of all subjects). $\mu \pm 2\sigma$ indicates that 95.5 % of the values lie within that range whereas 99.7 % of the values lie within $\mu \pm 2\sigma$ range.* ***B)*** *A histogram lag values (between all denoised tICA pairs of all subjects), with the mean lag of 0.0 s and standard deviation of 4.0 s.* ***C)*** *Correlation versus time lag scatterplots of three first nodes in the model order 30 and 50 tICA. The directionality of the leading DMN component is marked by triangle and circle symbols. Correlation values are absolute values. The line of $\mu \pm 3\sigma$ indicates the threshold of statistical significance validated in Figure 5A.*

Figure 6. *Subject variability in lag histograms (whole time window). The mean lag over subjects varies between -0.3…0.5s with standard deviation of 3.6...4.5.*

Figure 7. A) *Six histograms of correlation coefficients, presenting six time windows. In all time windows μ=0.00 and σ =0.25.* ***B)*** *The lag value histograms for six time windows. The mean lag is close to zero (-0.1..0.0) in all time windows with almost constant standard deviation (4.1-4.2) over all time windows.*

Figure 8. *Spatial distributions of subconnectivities in five control subjects. Those voxels whose VLF time signals correlates > 0.3 with tICA are color encoded, .i.e. red color indicating DMN_{pcc} and green DMN_{vmpf} areas. All images are shown in x=24, y=17, z=22 plane.*